THE ASTROPHYSICAL JOURNAL, 506:431–438, 1998 October 10

PHYSICAL STRUCTURE OF A CORONAL STREAMER IN THE CLOSED-FIELD REGION AS OBSERVED FROM UVCS/*SOHO* AND SXT/*YOHKOH*

J. LI[1] AND J. C. RAYMOND
Harvard-Smithsonian Center for Astrophysics, Cambridge, MA 02138
L. W. ACTON
Physics Department, Montana State University, Bozeman, MT 59717
J. L. KOHL
Harvard-Smithsonian Center for Astrophysics, Cambridge, MA 02138
M. ROMOLI AND G. NOCI
Universita di Firenze, I-50125, Firenze, Italy
AND
G. NALETTO
Università di Padova, I-35131, Padova, Italy
Received 1998 March 3; accepted 1998 October 10

ABSTRACT

We analyze a coronal helmet streamer observed on 1996 July 25 using instruments aboard two solar spacecraft, the Ultraviolet Coronagraph Spectrometer (UVCS) on board *Solar and Heliospheric Observatory* (*SOHO*) and the Soft X-Ray Telescope (SXT) on board *Yohkoh*. We derive temperatures and electron densities at 1.15 $R_\odot$ from SXT/*Yohkoh* observations. At this height, the streamer temperature is about $\log T\ (\mathrm{K}) = 6.28 \pm 0.05$, and the electron density is about $\log n_e(\mathrm{cm}^{-3}) = 8.09 \pm 0.26$, while at 1.5 $R_\odot$ a temperature of $\log T\ (\mathrm{K}) = 6.2$ and a density of $\log n_e(\mathrm{cm}^{-3}) = 7.1$ are obtained by UVCS/*SOHO*. Within the measurement uncertainty this suggests a constant temperature from the base of the streamer to 1.5 $R_\odot$. Electron density measurements suggest that the gas in the streamer core is close to hydrostatic equilibrium. Comparison with potential field models for the magnetic field suggests a plasma β larger than 1 in the closed-field region in the streamer. In deriving electron densities and temperatures from the SXT/*Yohkoh* data, we include the effects of abundance anomalies on the SXT filter response. We use the elemental abundances derived from the UVCS/*SOHO* observations to estimate the first ionization potential and gravitational settling effects. We then give the set of abundances for the solar corona, which agrees with our observations. In addition, we analyzed the SXT data from 6 consecutive days. We found that from 1996 July 22 to July 27, the physical properties of the streamer are nearly constant. We conclude that we may be observing the same loop system over 6 days.

Subject headings: Sun: corona — Sun: fundamental parameters — Sun: magnetic fields — Sun: X-rays, gamma rays

1. INTRODUCTION

During total solar eclipses, coronal streamers are seen as bright, narrow radial structures in white-light images (see, e.g., LASCO Daily Images). They also show threadlike and looplike fine structure (Koutchmy, Zirker, & Steinolfson 1991) and make up the irregular shape of solar corona, which varies with time. In SXT images these streamers usually overlie extended magnetic neutral lines—often the location of quiescent prominences.[2] Among these streamers, quiescent streamers are relatively stable and surround the solar equator, forming an equatorial streamer belt most apparent during solar minimum (see, e.g., Wang et al. 1997b). The streamers have lifetimes of several solar rotations, and they are not associated with other solar activities.

Pneuman & Kopp (1971) presented the first numerical MHD model of a streamer. Their model showed that a streamer consists of closed-field and open-field regions separated by a very thin current sheet. They also predicted that the temperature should be constant along the field lines in the closed-field region as the result of plasma equilibrium in the region. The closed-field region is characterized by hydrostatic equilibrium in the lower part of the corona, and the open-field region is characterized by a slow expanding state outside the closed-field region. Both white-light and X-ray images show many streamers having this type of configuration, though magnetic field models also suggest more complex structures, especially at low heights (see, e.g., Wang et al. 1997a). In further studies of the properties of the solar wind, it is found that the streamer plasma forms a part of the solar wind (Gosling et al. 1981; Feldman et al. 1981).

The existence of the solar wind was first proposed from the behavior of type I comet tails. It is the most observable feature of interplanetary space. The question arose, "where on the Sun does most of the solar wind plasma come from?" (Foukal 1990, p. 426). Since the solar wind was detected in the 1960s, it has been known that two forms of solar wind exist: slow- and fast-speed wind. The fast wind is clearly associated with coronal holes, while the slow wind is quite variable in terms of temperature, composition, and magnetic field strength (see, for instance, the review by Axford & McKenzie 1997). Elemental abundances in the center of the streamer (perhaps corresponding to the closed-field region of the streamer) and leg (corresponding to the

[1] Visiting Scientist, Smithsonian Astrophysical Observatory.
[2] Images and information regarding SXT calibration issues are available at http://www.lmsal.com/SXT/html/calibration.html.

open-field region) are similar to those in the slow solar wind (Raymond et al. 1997), which supports the identification of streamers as sources of the slow solar wind (see, e.g., Sheeley et al. 1997). The streamers will also help us answer one of the fundamental questions of the Sun: how is the solar corona heated? For instance, temperature structure in the streamers may indicate whether a heat source exists in the low or high corona (Suess, Wang, & Wu 1996; Wheatland, Sturrock, & Acton 1997), or whether the heating rate scales with density or magnetic field strength (Wang et al. 1997a). To better understand the solar wind and coronal heating problem, it is important to address a clear physical image of streamers.

Several studies of electron densities and temperatures in coronal streamers have been reported. Sturrock, Wheatland, & Acton (1996) studied a streamer with SXT/*Yohkoh* and found that the temperature varied with height in the closed-field region.[3] They concluded that there is no heat source below 1.5 $R_\odot$ and that the region is heated by nonthermal energy deposited beyond 1.5 $R_\odot$. Feldman et al. (1998), however, studied another quiescent streamer using emission-line data from SUMER/*SOHO* and instead found a constant temperature from 1.03 to 1.5 $R_\odot$. In our work, we compare the temperature at 1.15 $R_\odot$ measured from SXT/*Yohkoh* with the temperature at 1.5 $R_\odot$ measured from UVCS/*SOHO*.[4] We found the same temperature at two heights within the uncertainties at the two independent measurements.

Raymond et al. (1997) measured absolute elemental abundances in a quiescent streamer using UVCS. They found that the abundances not only are different from photospheric abundances but also vary within the streamer. The first ionization potential (FIP) effect, according to which elemental abundances depend on the FIP, is present. In the core of the streamer (near the equator at 1.5 $R_\odot$), oxygen and other high-FIP elements are depleted by 1 order of magnitude compared with photospheric abundances, while in the leg (about 40° from the equator) of the streamer they are depleted relative to the photospheric abundances by only a factor of 3. On the other hand, the low-FIP elements are found at nearly photospheric abundances in the streamer legs, but they are depleted in the streamer core by a factor of 3. Raymond et al. (1998) suggested gravitational settling in the closed-field region of the streamer core as the cause of this difference.

Schmelz, Saba, & Strong (1997) have compared the temperature distribution within an active region observed by SXT/*Yohkoh* and Solar Extreme-Ultraviolet Rocket Telescope and Spectrograph (SERTS). In their work, the SXT/*Yohkoh* response function was adjusted by replacing the Meyer (1985) elemental abundances with the coronal abundance set of Feldman (1992). In our paper, we discuss the effects of abundance anomalies derived from UVCS and SUMER on the interpretation of SXT/*Yohkoh* observations. We give the temperatures, densities, and gas pressure derived from the observations in the streamer in the closed field. We comment on the volumetric heating model of Suess et al. (1996) based on our observations.

[3] Information regarding *Yohkoh* is available at http://umbra.nascom.nasa.gov/yohkoh-archive.html.

[4] UVCS analysis software and data are available at http://cfa-www.harvard.edu/uvcs/.

2. DATA REDUCTION

The UVCS/*SOHO* observes the solar corona at elevations from 1.4 to 11 $R_\odot$ (Kohl et al. 1996). It observes solar coronal spectra in two wavelength channels: the OVI channel primarily covers the range 940–1123 Å (473–561 Å in second order); the LYA channel covers the range 1160–1350 Å. These two channels allow us to obtain absolute elemental abundances from the emission lines of several individual elements. SXT/*Yohkoh* (Tsuneta et al. 1991) is designed to observe the whole solar disk in the wavelength range from 3 to 45 Å. Its grazing incidence mirror is made unusually short for better performance of wide-field observations (Watanabe 1987). This allows us to use the data near the edge of the images without introducing intolerable errors. We compare the temperatures, electron densities, and pressure derived from observations of a streamer made from these two spacecraft.

We analyzed images obtained by SXT from 1996 July 22 through July 27. This period covered the streamer observed by UVCS/*SOHO* on 1996 July 25, which is the same streamer analyzed in Raymond et al. (1997). We concentrate on the base of the streamer on the west limb (Fig. 1, *rectangle*). It is typical of equatorial streamers observed during the first 6 months of the *SOHO* mission near solar minimum. The SXT telemetry constantly switches the observing mode among the filters taking dark frames, leak images (very important for the calibration because of entrance filter failures after 1992 November 14; L. Acton 1997, private communication), and the object images. The former two types of images are for calibration. We selected the SXT images with exposure times greater than 0.5 s. To derive temperatures, we used images taken within the same orbit through Al.1 and AlMg filters. For each selected image, the *Yohkoh* software package was applied to remove leaked stray light, to clean the specks (from CCD artifacts and cosmic rays), and to register the images spatially. Since the corona is very faint and the optical stray light was severe after the second entrance filter failed, we applied additional leak correction to each image. We normalized the leak images to a noncoronal signal area of each image and then subtracted. Finally, the images were summed to enhance the signal-to-noise ratio (S/N). Since the quiescent streamer was stable during the period of 1 day, we added all summed images of each orbit within 1 day together to again enhance the S/N. Therefore, we obtained the temperature, electron density, and gas pressure variations from day to day.

We extracted the signal from the SXT data in a rectangular region covering 1.08 to 1.24 $R_\odot$, as shown in Figure 1. We take 1.15 $R_\odot$ as our observing height for this region, the area of which corresponds to the base of the streamer that was observed by UVCS on 1996 July 25. The rectangle is located within the central region of the streamer. The statistical uncertainties of the measurement are very small; instead, systematic errors due to the method of stray light subtraction and theoretical spectral models dominate the error. From experiments with different methods of stray light subtraction and different sets of abundances, we estimate that the error in the log of the temperature is about ± 0.05 for the observation made on 1996 July 25 (the uncertainties of the temperatures for the other days were obtained using the same procedure). Uncertainty of the emission measure (EM) could be derived from the uncer-

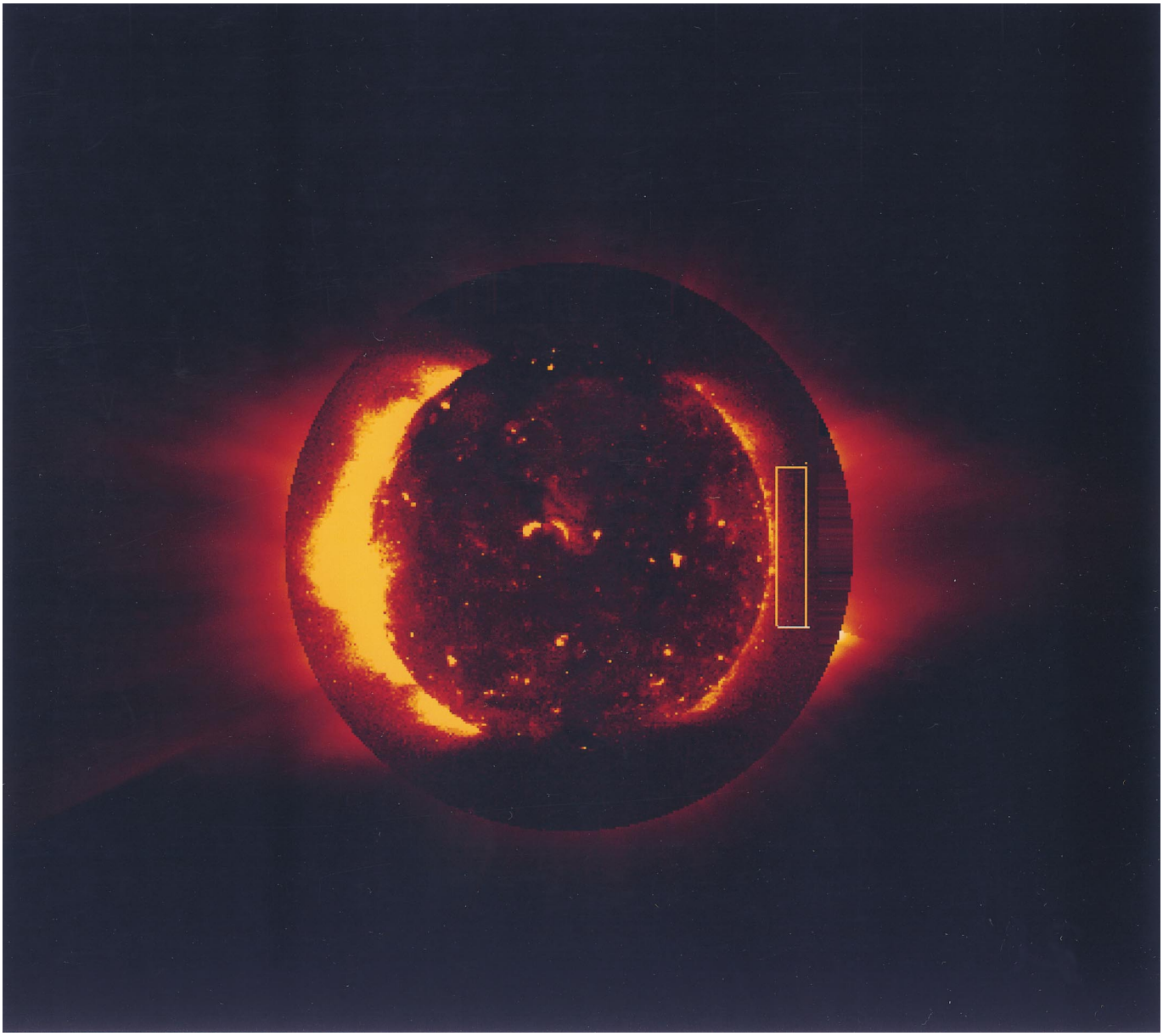

FIG. 1.—Solar disk images from both SXT/*Yohkoh* (*inner*) and UVCS/*SOHO* (*external*) on 1996 July 25. The box indicates the observed area with SXT data covering 75″ × 380″. The area ranges from 1.08 to 1.24 $R_\odot$. The UVCS image was obtained with OVI $\lambda\lambda$1032 and 1037. It combined the daily UVCS synoptic scans with additional spectra. The image consists of observations from heights 1.4, 1.5, 1.6, 1.7, 1.85, 2.0, 2.25, 2.5, 3.0, 3.5, and 4.0 $R_\odot$. The two legs of the streamer are clearly seen in this image on the west limb (see also Raymond et al. 1997).

tainty of temperature. In turn, uncertainties regarding electron density and gas pressure could be derived from EM uncertainty using the corresponding relations. We will give those uncertainties, along with the measured values, in the following sections.

3. ANALYSIS

Our objective is to measure the EM, electron temperature, electron density, and gas pressure in the streamer at heights of 1.15 and 1.5 $R_\odot$. We demonstrate that the independent measurements from both SXT and UVCS data are consistent.

3.1. *Elemental Abundances*

We found that the different sets of abundances have visible effects on the EM and temperatures derived from SXT data. In turn, the electron densities and gas pressures are affected. The abundances of He, N, O, Ne, Mg, Al, Si, S, and Fe were determined with UVCS/*SOHO* at 1.5 $R_\odot$ in the streamer (Raymond et al. 1997, Table 7, streamer center). Among these elemental abundances, only upper limits of He, N, and Ne were given by UVCS. The uncertainty of the abundances of other elements is about 20%. Therefore, we have some constraints on elemental abundances with UVCS observations in the streamer at 1.5 $R_\odot$.

To compose reasonable elemental abundances in the streamer at 1.15 $R_\odot$, first we grouped elements according to their low- and high-FIP state. We interpolated the abundances of high-FIP elements between 1.0 and 1.5 $R_\odot$ based on oxygen abundances at 1.03 $R_\odot$ (6.2×10^{-4}) determined by SUMER/*SOHO* (Feldman et al. 1998) and at 1.5 $R_\odot$ (6.3×10^{-5}) determined by UVCS. We interpolated the low-FIP elemental abundances based on the abundances of Fe, 4.86×10^{-5} at the base of the streamer, and 1.0×10^{-5} at 1.5 $R_\odot$ obtained by UVCS. Second, as the low-FIP

element abundances are enhanced at the chromosphere (Meyer 1985), we enhanced each low-FIP elemental abundance at the base of the streamer by a factor of 3. Third, we used the mass dependence suggested by Feldman et al. (1998) to reduce the abundances of heavy elements such as Ar, Ca, Fe, and Ni by a factor of 2 above the solar surface. Using these steps, we could obtain elemental abundances at any height in the closed-field region in the streamer. We could also obtain abundances of elements for which UVCS did not provide constraints. For instance, the abundance of carbon was derived by interpolation assuming that it is a high-FIP element and has photospheric abundance of 8.62. The photospheric abundances and those at the streamer's base, at 1.15 and 1.5 $R_\odot$ obtained by the interpolation, are shown in Table 1. To compare the elemental abundances in our work with those applied in the SXT standard routine (Mewe, Gronenschild, & van den Oord 1985; Meyer 1985), we list the abundances used by SXT in Table 1, as well.

3.2. *Electron Temperature and Density from SXT*

The derivation of temperatures and EM depends on knowledge of the spectrum emitted by a hot plasma of given elemental abundances and equilibrium ionization balance. Theoretical X-ray spectra from 1 to 300 Å were calculated for temperatures $5.5 \leq \log\ (T) \leq 8.5$ using the current version of the Raymond & Smith (1977) code. The number of photons per second emitted by the hot plasma and detected by SXT was calculated by combining theoretical spectra with the SXT effective area and integrating along the line of sight (LOS):

$$\text{photon rate} = \int \frac{\varepsilon(\lambda) n_e n_{\rm H} \lambda A_e(\lambda)}{4\pi(\text{AU})^2 hc}\, dv\, d\lambda \qquad (1)$$

where the photon rate is the number of photons s^{-1}, $\varepsilon(\lambda) n_e n_{\rm H}$ is theoretical emissivity (ergs cm^{-3} s^{-1}), $A_e(\lambda)$ is the SXT effective area, AU is the astronomical unit measured in centimeters, h is Planck's constant, dv is an element of volume in the LOS, and c is the speed of light. Separating the volume integration from the wavelength integration, we obtain the number of photons as a function of the EM, which we define as $\text{EM} = \int n_e n_{\rm H}\, dv$. The conversion from absorbed energy to data number (DN) for SXT is 365 eV DN^{-1} (Tsuneta et al. 1991).

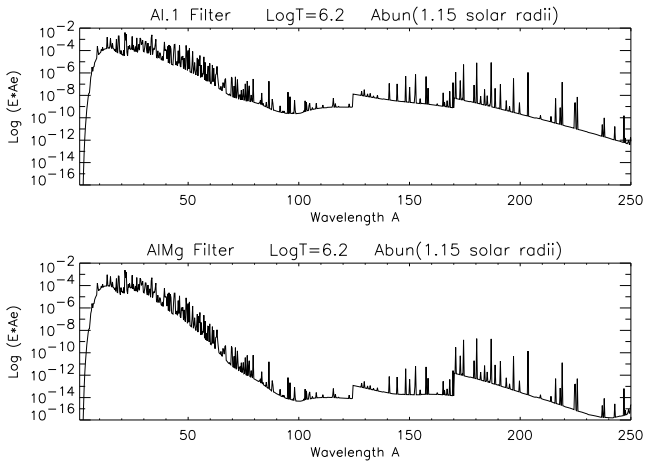

FIG. 2.—Combination of theoretical X-ray emission line spectra by Raymond & Smith (1977) with SXT effective area with filters Al.1 and AlMg. The spectrum is calculated with $\log\ T\ (\text{K}) = 6.2$. The x-axis is wavelength and the y-axis is X-ray emissivity multiplied by SXT effective area in log.

We computed theoretical X-ray spectra using the elemental abundances described above. The combination of the spectra with the SXT/*Yohkoh* effective area is shown in Figure 2. Figure 3 shows the SXT response functions (data numbers s^{-1}) as a function of $\log T$ for both Al.1 and AlMg filters (for comparison, the standard SXT/*Yohkoh* response functions for the same two filters are dashed lines). The ratio of data numbers s^{-1} from AlMg and Al.1 filters is shown in Figure 4. We derive the temperature with this curve for a given measured data number ratio. The EM is derived using Figure 3 for a given temperature. For comparison, Figure 5 gives the temperatures and EM obtained by both the

TABLE 1

ELEMENTAL ABUNDANCES

Element	FIP state	Photosphere[a]	1.0 $R_\odot$[b]	1.15 $R_\odot$[b]	1.5 $R_\odot$[b]	SXT[c]
H	...	12.0	12.0	12.0	12.0	12.0
He	High	10.99	10.88	10.74	9.86	10.99
C.....	High	8.62	8.51	8.37	7.49	8.37
N	High	8.0	7.89	7.75	6.87	7.59
O	High	8.93	8.82	8.68	7.80	8.39
Ne	High	8.11	8.00	7.86	6.98	7.55
Mg.....	Low	7.58	8.26	8.14	7.55	7.57
Si	Low	6.47	8.23	8.11	7.52	7.59
S	High	7.55	7.10	6.96	6.08	6.94
Ar.....	High	7.21	6.24	6.10	5.22	6.33
Ca	Low	6.65	6.73	6.61	6.03	6.47
Fe.....	Low	7.51	7.88	7.76	7.18	7.59
Ni.....	Low	6.25	6.62	6.50	5.92	6.33

[a] Photospheric abundances adopted from Feldman 1992.

[b] Abundances are derived from Fe and O depending on low- and high-FIP elements. For the low-FIP elements, the abundances were derived from the slope of Fe, which was determined at 1.5 $R_\odot$ by UVCS and was assumed as 1.62×10^{-5} at 1.03 $R_\odot$. The O abundances are 6.2×10^{-4} at 1.03 $R_\odot$ (by SUMER) and 6.3×10^{-5} at 1.5 $R_\odot$ (by UVCS). At the streamer's base (1.0 $R_\odot$), the heavy low-FIP elements have higher abundances relative to the photospheric abundances due to the low-FIP enhancement effect.

[c] Elemental abundances applied by the SXT standard routine (Mewe et al. 1985; Meyer 1985).

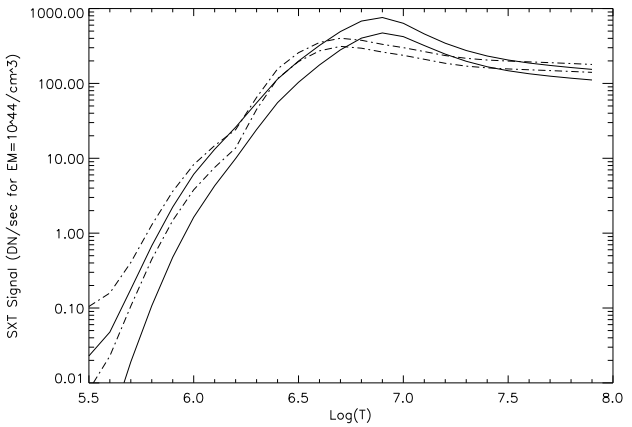

FIG. 3.—SXT signal measured in data numbers as a function of log T. The solid lines are response functions with the Raymond & Smith (1977) X-ray spectral model. The dashed lines are response functions with the Mewe et al. (1985; 1986) model. For each pair of curves, the upper is Al.1, and the lower is AlMg.

Raymond & Smith (1977) code (from present work) and the SXT standard routines (Mewe et al. 1985; Mewe, Lemen, & van den Oord 1986). Differences between the X-ray models are discussed in § 4.

We calculate the electron density from the EM under the assumption of hydrostatic equilibrium, which gives electron density at height r,

$$n_e(r) = n_e(r_0) \exp\left[-\frac{\mu m_H GM\ R_\odot}{kTr_0}\left(1-\frac{r_0}{r}\right)\right], \quad (2)$$

where $n_e(r_0)$ is the density at the height at which the observation was taken, the average mass is $\mu = 0.6$, m_H is the atomic mass unit, G is the gravitational constant, $M_\odot$ is the solar mass, k is Boltzmann's constant, and T is the temperature. The electron density (n_e) and hydrogen density (n_H) have the relation $n_e = 1.10 n_H$ for the low He abundance at 1.15 $R_\odot$ (0.05; see Table 1). We assume that the temperature is constant along the LOS and the integral is for a

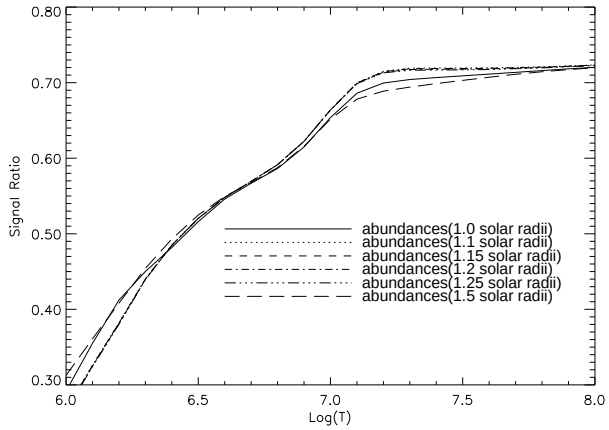

FIG. 4.—Ratio of AlMg/Al.1 as a function of log T. The curve is plotted based on the Raymond & Smith (1977) X-ray spectral model. The six curves represent six sets of abundances used in the theoretical spectral computation. The set of abundances are derived using the interpolation method described in § 3.1 and are functions of the height.

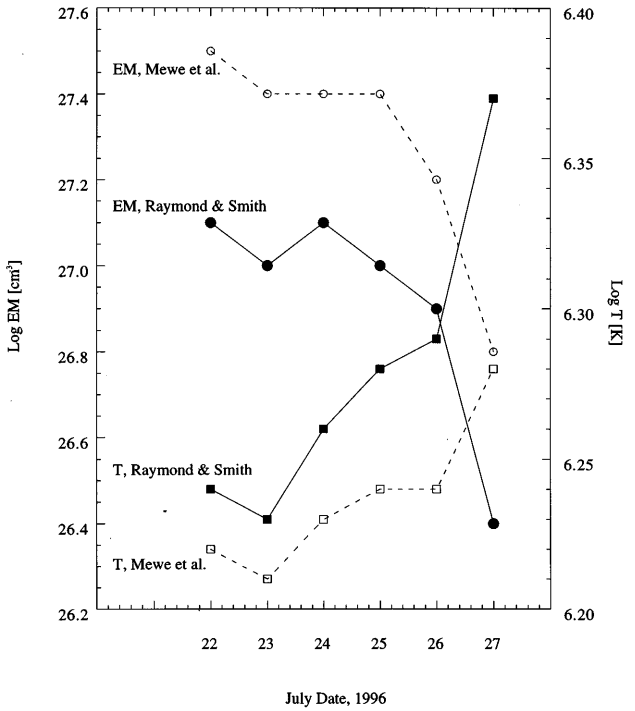

FIG. 5.—Comparison of log T and log EM measured by Raymond & Smith (1977) (current work) and the Mewe et al. (1985; 1986) model (the standard spectral model used by SXT/*Yohkoh* data reduction IDL package). Note that Mewe et al. (1985; 1986). EM values have been converted to our definition of EM. The observations were made on 1996 July 22–27.

spherically symmetric corona, and we solve to find

$$n_e(r_0) = \sqrt{\frac{1.10\ \mathrm{EM}}{r_0 I}}, \quad (3)$$

where $I = \int \exp\{-(2\mu m_H GM\ R_\odot/kTr_0)[1-(r_0/r)]\}d\ell$ is the integral length along the LOS. The electron density is derived from EM as well as the integral length by using equation (3). Besides the uncertainty caused by EM measurement, the errors of integral length also affect electron density accuracy. The integral uncertainty along the LOS caused by temperature uncertainty is about 23% for the streamer on 1996 July 25. The integral lengths (I) are between 0.8 and 1.0 $R_\odot$ for the streamer on 1996 July 22–26. The length on 1996 July 27 is 2.05 $R_\odot$. The large difference of integrals between the streamer on 1996 July 27 and the streamers on other dates was caused by the temperature difference (see Fig. 5).

On the other hand, the temperatures are constant within uncertainties in the streamers from 1996 July 22 to July 26 (Fig. 5). However, the constant temperature over the time observed may have lasted even longer based on the similarity of UVCS synoptic images. We assume that these streamers belong to the same magnetic loop system. From LASCO C2 images that each cover from 1.5 to 6.0 $R_\odot$, we noticed that a single bright triangle-shaped streamer was on the west limb from 1996 July 22 through July 27. Both before 1996 July 22 and after 1996 July 27, the shape of the streamer had changed. This supports the assumption that the structure is uniform over the region that contributes to the observed fluxes.

Figure 6 plots electron density as a function of $r/R_\odot$ at $T = 1.58 \times 10^6$ K under hydrostatic equilibrium (*solid line*).

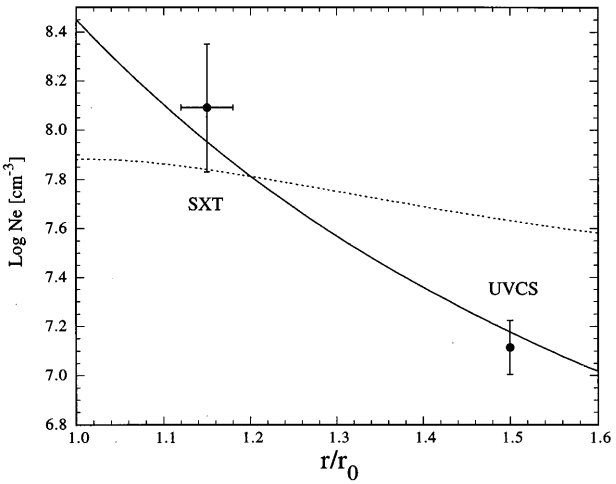

FIG. 6.—Comparison of measured electron densities at 1.15 and 1.5 $R_\odot$ (*filled circles* marked by SXT and UVCS, respectively) with hydrostatic equilibrium model (*solid line*) curve. The observations were made on 1996 July 25. The dashed line indicates a hydrostatic equilibrium plus thermal conduction. Both curves are plotted with a constant temperature log T (K) = 6.2. In this plot, the density at the solar surface is adjusted so that the curve fits measured densities.

The electron densities obtained from SXT and UVCS on 1996 July 25 are marked on the graph at heights of 1.15 (from SXT) and 1.5 $R_\odot$ (from UVCS). Taking into account a streamer's unknown three-dimensional structure and uncertainties caused by EM measurements, we estimate the uncertainty on electron density is about ± 0.26 in log n_e from the SXT measurement. We will discuss this graph further in § 4. For comparison, we plot the electron density as a function of $R_\odot$ assuming thermal conduction dominates (Lang 1980, p. 287) in Figure 6 (*dashed line*).

We calculated gas pressure from the electron density using the relation $P = (n_e + n_H)kT$ [dyn cm^{-2}], where k is Boltzmann's constant, T is the electron temperature, and n_e and n_H represent the electron and ion density. For the streamer on 1996 July 25 we obtained the following physical parameters at 1.15 $R_\odot$: the temperature is log T (K) = 6.28 ± 0.05; the EM is log EM (cm^{-3}) = 27.05 ± 0.33; the electron density is log n_e (cm^{-3}) = 8.09 ± 0.26; and the gas pressure is 0.06 ± 0.02 dyn cm^{-2}. We will compare these parameters with those from UVCS in § 4.

3.3. *Electron Temperature and Density from UVCS*

The temperature at 1.5 $R_\odot$ was derived from UVCS observations in two ways (Raymond et al. 1997). The electron temperature was found from the relative concentrations of different ions of several elements, along with theoretical ionization balance calculations (Arnaud & Rothenflug 1985; Arnaud & Raymond 1992). The result was log $T = 6.2$. It is difficult to know the uncertainty in the theoretical ionization balance, but a typical estimate is 0.1 in log T (Raymond 1998). The proton temperature can be derived more directly from the Doppler width of the Lyα line (thanks to the tight coupling between neutral and ionized hydrogen by charge transfer). Again the result was log $T = 6.2$. The equality of electron and proton temperatures indicates that the relatively high-density plasma in streamers is collisionally coupled, at least at this modest height (see also Noci et al. 1997; Kohl et al. 1997).

Electron densities were not given in Raymond et al. (1997), but they follow directly from that analysis (Romoli & Fineschi 1994). The Lyman lines are made up of collisionally and radiatively excited components. Comparison of the theoretical intensity ratio $I(\text{Ly}\beta)/I(\text{Ly}\alpha)$ with the predicted values for collisional and radiative excitation yields collisional excitation fractions for Lyβ of 57% in the streamer core and 47% in the streamer leg (Raymond et al. 1997, Table 4). These values must equal

$$\frac{I_{\text{coll}}}{I_{\text{rad}}} = \frac{\int n_e n_H q_{\text{ex}}\, dl}{\int n_H \sigma I_0 W\, dl} \tag{4}$$

along the LOS. Here q_{ex} is the effective Lyβ collisional excitation rate coefficient (including the branching ratio and the recombination contribution; Raymond et al. 1997), σ is the radiative scattering cross section that depends on the kinetic temperature and (weakly) on the chromospheric emission profile, I_0 is the disk Lyβ intensity, and W is the dilution factor as a function of height. The line-of-sight integration requires some knowledge of the radial dependence of the density. Observations of the same streamer above 1.5 $R_\odot$ can be matched by $n_e \propto R^{-4}$ (Raymond et al. 1998), so we use that dependence to evaluate the integrals and derive $n_e = 1.3 \times 10^7$ and 8.5×10^6 cm^{-3} in the center and the leg of the streamer, respectively (note that these densities supplant the earlier estimates given by Raymond et al. 1998). The uncertainty includes errors in atomic rates, instrumental calibration, and integration, and it is probably 20%–30%. The spectrograph slit actually crossed the streamer core at 1.50 $R_\odot$ and the leg at about 1.58 $R_\odot$. If $n \propto R^{-4}$ is an accurate approximation, the density in the leg at 1.5 $R_\odot$ is $\sim 1.1 \times 10^7$ (cm^{-3}), which is within the uncertainty of the streamer-center value.

4. DISCUSSION

The effect of gravitational settling is considered in our work by reducing the abundances of heavy elements in the low streamer (as described in § 3.1).

We have measured temperatures and EM from SXT data based on the theoretical X-ray emission line spectra by Raymond & Smith (1977). For comparison, we obtained T and EM using standard SXT routines based on the theoretical spectra of Mewe et al. (1985). We plotted these measurements with both models in Figure 5. The temperatures agree with each other within the uncertainties in both models; however, the EM are smaller by 0.3–0.4 in log EM with the model by Raymond & Smith (1977) than with the SXT standard model. One factor is that Raymond & Smith (1977) included predicted emission from weak emission lines in an effort to describe the total rate, while Mewe et al. (1985) concentrated on lines strong enough to be individually observed. Raymond & Smith (1977) also included estimates of the cascade and resonance contributions to the excitation cross sections even when these estimates are quite uncertain. In Figure 3, a kink appears at log $T \approx 6.2$–6.3 in SXT standard response function, while the curves are smooth in the response functions with the code of Raymond & Smith (1977). This may be because of the use of a different ionization balance. The third factor is that Mewe et al. (1985) defined the EM as $\int n_e^2\, dv$, while Raymond & Smith (1977) defined the EM as $\int n_e n_H\, dv$. Finally, some of the different results from the different abundance sets are assumed. All these factors caused the values of EM inferred

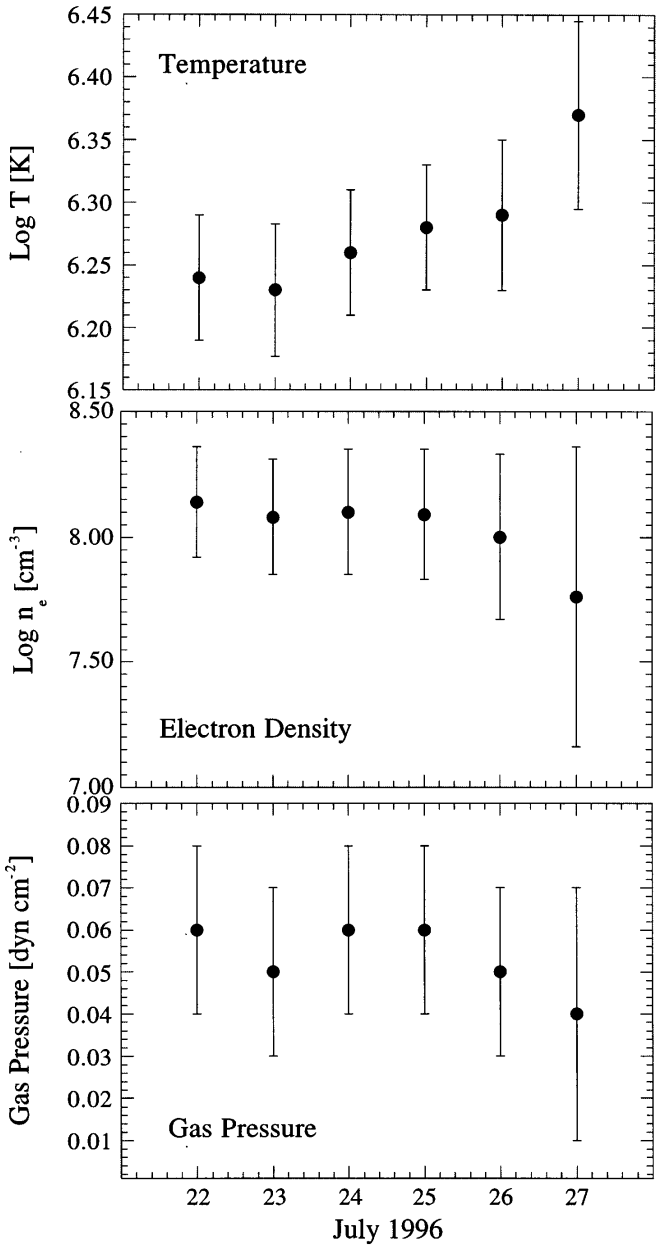

FIG. 7.—Measured temperatures, electron densities, and gas pressure varying with the days. The measurements were made from SXT. Note that these three physical parameters are nearly constant over 6 days within uncertainties.

from the Raymond & Smith (1977) model to be smaller than those from the Mewe et al. (1985) model.

We derived log T (K) = 6.28 ± 0.05 from SXT data at 1.5 $R_\odot$ on 1996 July 25. Within the uncertainty, the temperature agrees with the value at 1.5 $R_\odot$, log T (K) = 6.2, obtained by UVCS. This supports the result of Feldman et al. (1998) based on SUMER measurements that the temperature is constant in the streamer core. The electron density measurements from SXT and UVCS are shown in Figure 6. Along with the 1.58×10^6 K hydrostatic equilibrium curve (*solid line*), we mark the measured electron densities at both 1.15 and 1.5 $R_\odot$. The two measured densities agree reasonably well with the solid line. This supports the hypothesis that the streamer is in hydrostatic equilibrium and isothermal in the closed-field region, but does not contradict the model of Noci et al. (1997), which has very low speeds near the base of this streamer.

Suess et al. (1996) described a coronal streamer model having a volumetric heating source and thermal conduction. In their model, no steady state is achieved in the streamer with the existence of a heat source. What actually happens is that the magnetic field lines are constantly stripped from the top of the streamer and opened to the interplanetary medium. This comes about because the ratio of thermal pressure to magnetic pressure, $\beta \equiv P_{\rm gas}/(B^2/8\pi)$, is much larger than unity (as large as 20) in the core of the streamer, while β is less than unity in the outer sheath. We obtain the gas pressure for our streamer as 0.06 ± 0.02 (dyn cm^{-2}) at 1.15 $R_\odot$ and 0.006 (dyn cm^{-2}) at 1.5 $R_\odot$. The magnetic field strength is about 0.55 G at 1.15 $R_\odot$ and 0.21 G at 1.5 $R_\odot$ according to a potential field calculated by A. van Ballegooijen (1998, private communication; see Raymond et al. 1998). The extrapolation of the magnetic field is based on NSO/Kitt Peak synoptic maps of the radial magnetic fields for the month of 1996 July, along with the assumption of a source surface (radial field) at 2.5 $R_\odot$ (Schatten, Wilcox, & Ness 1969). This, of course, makes the potential field calculation suspect. We compared the potential field with the configuration given by Suess et al. (1996) based on an MHD calculation, since our plasma β depends upon the magnetic field. The topology of the magnetic field shown in Suess et al. (1996) has a narrow arch shape in the closed-field region of the streamer, while the potential field model predicts too wide a streamer. The Suess et al. (1996) magnetic field configuration is closer to the observed streamer images than that of the potential field. The total magnetic fluxes are the same from both models, and there is no fundamental difference between the extrapolated potential field and the Suess et al. (1996) MHD model. We note, however, that neither model would give a flux rope along the neutral line, as might arise from shear along the neutral line.

Our measurements imply that β is 5 at 1.15 $R_\odot$ and 3 at 1.5 $R_\odot$ in the closed-field region, which is greater than unity, although the exact values are uncertain because of the uncertainty in the coronal magnetic field. Our current work supports the streamer model suggested by Suess et al. (1996) in several aspects:

1. The gas pressure is important in the closed-field region as the plasma β is greater than unity (though smaller than predicted by Suess et al. 1996), and it may cause the magnetic field lines to be stripped from the top of the streamer.
2. The plasma β is greater at lower heights (5 at 1.15 $R_\odot$) than at higher heights (3 at 1.5 $R_\odot$) of the streamer. This agrees with the Suess et al. (1996) model that β is very high in the deep core of a streamer and that it decreases as the elevation of the streamer increases.
3. A direct result of adding thermal conduction in the Suess et al. (1996) model is that temperature is somehow averaged in a large range of radii. The constant temperature from 1.15 to 1.5 $R_\odot$ that we discovered from our work may indicate the existence of thermal conduction in the closed-field region.

However, our work shows some opposition to the Suess et al. (1996) model. First, they suggested that the temperature in the streamer core could reach temperatures as high as 3.5×10^6 K. The temperature obtained in the current work is about 1.6×10^6 K, which suggests a smaller heating rate

than that assumed by Suess et al. (1996). To examine the importance of thermal conduction, we plot electron density as a function of height in a hydrostatic equilibrium plus thermal conduction (Lang 1980, p. 287; *dashed line*) in Figure 6. The measured densities are consistent with the hydrostatic equilibrium with a constant temperature within uncertainties, but less with this conductive model.

We used the same analysis to obtain the physical parameters for the streamers on the west limb from 1996 July 22 to July 27. We see that temperatures, electron densities, and gas pressure are almost constant within uncertainties (Fig. 7). There is no obvious reason that streamers should have similar physical conditions since they are isolated by magnetic loops; however, we may imagine that we measured the same magnetic loop system that supports these streamers from 1996 July 22 to July 27.

5. SUMMARY

We measured electron temperatures and EM and calculated densities and gas pressure of streamers appearing on the west limb of the solar disk on 1996 July 22–27. We compared these parameters at 1.15 and 1.5 $R_\odot$ from observations made by SXT and UVCS. We found a temperature constant with height, which agrees with the SUMER observation of a different streamer made by Feldman et al. (1998). The electron densities at these two heights are consistent with hydrostatic equilibrium. We calculated plasma β based on the measured gas pressure and an extrapolated magnetic field. Plasma β is greater than unity, which supports the conclusion of Suess et al. (1996) that the gas pressure is important in the closed-field region. Our observation suggests that the streamer is close to hydrostatic equilibrium and is isothermal.

On 6 consecutive days, we see only very small changes in the densities, temperatures, and gas pressure. We think that the streamers are supported by the same magnetic loop system along the solar magnetic equator for the first 6 days.

We are grateful to Tom Metcalf for helping with the data reduction and S. Suess for helpful discussions. We thank S. Fineschi, L. Gardner, A. Ciaravella, J. Michels, R. O'Neal, and R. Suleiman for their work on the calibration and operation of UVCS. J. L. and J. C. R. were supported by NASA grants NAG 5-3192 and NAG-528 to the Smithsonian Astrophysical Observatory. The work of L. W. A. was supported by NASA under contract NAS 8-40801. *Yohkoh* is a mission of ISAS in Japan. We thank Rita Johnson for help with obtaining SXT data.

REFERENCES

Arnaud, M., & Raymond, J. 1992, ApJ, 398, 394
Arnaud, M., & Rothenflug, R. 1985, A&AS, 60, 425
Axford, W. I., & McKenzie, J. F. 1997, in Cosmic Winds and the Heliosphere, ed. J. R. Jokipii, C. P. Sonett, & M. S. Giampapa (Tucson: Univ. Arizona Press), 33
Feldman, U. 1992, Phys. Scr., 46, 202
Feldman, U., Schuhle, U., Widing, K. G., & Laming, J. M. 1998, ApJ, submitted
Feldman, W. C., Asbridge, J. R., Bame, S. J., Fenimore, E. E., & Gosling, J. T. 1981, J. Geophys., 86, 5408
Foukal, P. 1990, Solar Astrophysics (New York: Wiley)
Gosling, J. L., Borrini, G., Asbridge, J. R., Bame, S. J., Feldman, W. C., & Hansen, R. T. 1981, J. Geophys., 86, 5438
Kohl, J. L., et al. 1996, Sol. Phys., 162, 313
———. 1997, Sol. Phys., 175, 613
Koutchmy, S., Zirker, J. B., & Steinolfson, R. S. 1991, in Solar Interior and Atmosphere, ed. A. N. Cox, W. C. Livingston, & M. S. Matthews (Tucson: Univ. of Arizona Press), 1044
Lang, K. R. 1980, Astrophysical Formulae (2d corr. enl. ed.; Berlin: Springer), 287
Mewe, R., Gronenschild, E. H. B. M., & van den Oord, G. H. J. 1985, A&AS, 62, 197
Mewe, R., Lemen, J. R., & van den Oord, G. H. J. 1986, A&AS, 65, 511
Meyer, J.-P. 1985, ApJS, 57, 173
Noci, G., et al. 1997, preprint
Pneuman, G. W., & Kopp, R. A. 1971, Sol. Phys., 18, 258
Raymond, J. C., et al. 1997, Sol. Phys., 175, 645
Raymond, J. C., & Smith, B. W. 1977, ApJS, 35, 419
Raymond, J., Suleiman, R., van Ballegooijen, A., & Kohl, J. 1998, in Proc. ESLAB Symp. 31, ed. A. Wilson, ESA SP415 (Noordwijk: ESA), in press
Romoli, M., & Fineschi, S. 1994, Space Sci. Rev., 70, 359
Schatten, K. H., Wilcox, J. W., & Ness, N. F. 1969, Sol. Phys., 9, 442
Schmelz, J. T., Saba, J. L. R., & Strong, K. T. 1997, BAAS, 29, 2
Sheeley, N. R., et al. 1997, ApJ, 484, 472
Sturrock, P. A., Wheatland, M. S., & Acton, L. W. 1996, ApJ, 461, L115
Suess, S. T., Wang, A.-H., & Wu, S. T. 1996, J. Geophys. Res., 101, 19957
Tsuneta, S., et al. 1991, Sol. Phys., 136, 37
Wang Y.-M., et al. 1997a, ApJ, 485, 419
———. 1997b, ApJ, 485, 875
Watanabe, T. 1987, Bull Tokyo Astron. Obs., 2, 277, 3213
Wheatland, M. S., Sturrock, P. A., & Acton, L. W. 1997, ApJ, 482, 510